ARTICLE

Chinese Journal of Structural Chemistry

Explicating the Role of Metal Centers in Porphyrin-Based MOFs of PCN-222(M) for Electrochemical Reduction of CO_2

Mengjie Liu[1†], Mengting Peng[1†], Baoxia Dong[1*], Yunlei Teng[1], Ligang Feng[1] and Qiang Xu[1*]

[1]*School of Chemistry and Chemical Engineering, Yangzhou University, Yangzhou, Jiangsu 225002, China*

ABSTRACT The porphyrin-based MOFs formed by combining Zr_6 clusters and porphyrin carboxylic acids with clear M-N_4 active centers show unique advantages in electrocatalytic reduction of CO_2 (CO_2RR). However, its conductivity is still the bottleneck that limits its catalytic activity due to the electrical insulation of the Zr cluster. Therefore, the porphyrin-based MOFs of PCN-222(M) (M = Mn, Co, Ni, Zn) with explicit M-N_4 coordination were combined with the highly conductive material carbon nanotube (CNT) for discussing the influence of metal centers on the CO_2RR performance based on theoretical calculations and experimental observations. The results show that the PCN-222(Mn)/CNT, PCN-222(Co)/CNT, and PCN-222(Zn)/CNT all exhibit high selectivity to CO (FE_{CO} > 80%) in the range of -0.60 to -0.70 V vs. RHE. The FE_{COmax} of PCN-222(Mn)/CNT (-0.60 V vs. RHE), PCN-222(Co)/CNT (-0.65 V vs. RHE), and PCN-222(Zn)/CNT (-0.70 V vs. RHE) are 88.5%, 89.3% and 92.5%, respectively. The high catalytic activity of PCN-222(Mn)/CNT and PCN-222(Co)/CNT comes from the excellent electron mobility of their porphyrin rings and their low ΔG_{*COOH} (0.87 and 0.58 eV). It reveals that the strength of backbonding π of the transition metal and its influence on the electron mobility in the porphyrin ring can affect its CO_2RR activity.

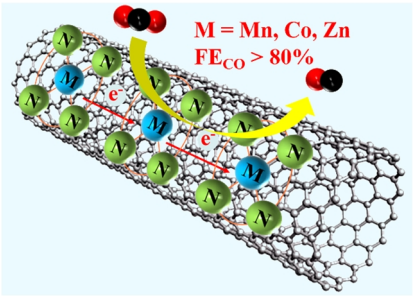

Keywords: PCN-222, electrochemical reduction of CO_2, DFT calculation, MOFs

n INTRODUCTION

The rapid economic development has increased the global demand for fossil fuels and produced excessive CO_2, which has led to problems such as energy crisis, global warming, etc.[1] To solve these problems, many methods have been explored to capture and utilize CO_2.[2-4] The electrocatalytic reduction of CO_2 (CO_2RR) has a potential application prospect due to its simple device and mild conditions.[5] A variety of electrocatalysts, including metal/metal oxide, molecular-based catalysts, carbon-based materials and so on for CO_2RR have been developed.[6-8] Among them, metal-doped nitrogen-carbon (M-N-C) materials are currently one of the most promising catalysts which were usually obtained through the pyrolysis process.[9,10] The combination of nitrogen atoms and carbon structures can form different chemical functional groups, including pyrrole N, graphite N, pyridine N, etc., and metal atoms can coordinate with them, creating potential M-N_x sites for CO_2RR.[11] However, their chemical structure needs to be characterized by X-ray absorption fine structure (XAFS), and the influence of other types of functional N and inorganic metal impurities cannot be excluded, which is not conducive to the study of the reaction mechanism.[12]

Metalloporphyrins, as molecular catalysts with definite M-N_4 structure, are extensively used in CO_2RR because their macrocyclic conjugated electron system is beneficial to electron migration.[13-15] It is revealed that M-N_4 is the most likely active site. However, this kind of catalyst is usually used in a homogeneous system, and its catalytic activity is often limited by its solubility in the solution.[16] Since the heterogeneous system can better control the chemical environment of the catalyst's active site, it is a meaningful subject to explore the application of porphyrin-based molecular catalysts in the heterogeneous system.[17-19]

Metal-organic framework (MOF) is a kind of porous material assembled by metal nodes and organic ligands, with the advantages of adjustable pore size and functionality, high specific surface, which may provide a suitable catalytic environment for the CO_2RR.[20] Porphyrin-based MOFs formed by connecting metalloporphyrin-based carboxylate with Zr_6/Zr_8 clusters in a high oxidation state have become an ideal choice for discussing CO_2RR activity with M-N_4 center, which also brings out a high hydro-stability,[21-28] such as PCN-222,[22] PCN-221,[23] PCN-224,[24] and so forth. In our previous work, we have proved that PCN-222(Fe) has a high selectivity of 91% for transforming CO_2 to CO.[29] In addition, we also discussed the influence of topological structure on the CO_2RR activity with PCN-222 (Cu) and PCN-224 (Cu) as models.[30] We found that PCN-222(Cu) with a tubular structure and a diameter of 3.2 nm showed a higher mass transfer rate and higher current density, achieving electron transfer more quickly.

As established by Hod et al., the redox jump on these periodically arranged and chemically equivalent sites—metalloporphyrins is the way of electron conduction in porphyrin-based MOFs.[31] Recently, they have investigated iron porphyrin-based MOFs formed by the same Zr_6 node and free TCPP(Fe^{III}) ligand (tetrakis (4-carboxyphenyl) porphyrinato iron(III)) with different topological structures, that is, PCN-222(Fe) (csq), MOF-525(Fe) (ftw), NU-902(Fe) (scu), and PCN-225(Fe) (sqc), on the redox jump rate (k_{hop}).[32] The results showed that in PCN-222(Fe), the redox jump path is in the direction of the hexagonal tubular channel along the *c*-axis. When the metal center of Fe coordinates with 1-methylimidazole (MIM) to form a six-coordinated low spin TCPP(Fe)/MIM complex, the k_{hop} in the redox jump process and the current density increase significantly, indicating that the charge transport is improved. Given this, in the same topological structure, changing the active metal center would have an impact on the redox jump

DOI: 10.14102/j.cnki.0254-5861.2022-0057

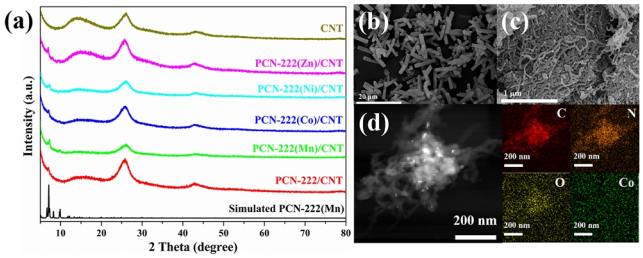

Figure 1. (a) PXRD patterns of CNT, PCN-222/CNT, and PCN-222(M)/CNT; SEM images of PCN-222(Co) (b) and PCN-222(Co)/CNT (c); (d) HAADF-STEM and EDS elemental mappings of PCN-222(Co)/CNT.

rate and even the catalytic activity of the extended system.

Nevertheless, the conductivity and catalytic activity of porphyrin-based MOFs are limited by the electrically insulated Zr clusters. Herein, the highly conductive material of carbon nanotube (CNT) was employed to combine with PCN-222(M) (M = Mn, Co, Ni, Zn) and PCN-222 (without metal center). With the aid of density functional theory (DFT) calculation and electrocatalytic measurement, we will reveal the CO_2RR mechanism and clarify the relationship between structure and catalytic activity.

n RESULTS AND DISCUSSION

Characterizations of PCN-222(M). The series of porphyrin-based MOFs were structurally characterized by IR, PXRD, and XPS (Figure S1-S4, ESI). The PXRD shows that the diffraction peak of the as-synthesized sample is consistent with the simulated one on the basis of the reported single-crystal diffractions, indicating that the prepared material is the target product and has good crystallinity. XPS results indicate that the corresponding metal center's oxidation states are Mn^{3+}, Co^{2+}, Ni^{2+} and Zn^{2+}, respectively (Figure S3, ESI). The fitted high-resolution N1s spectra further prove the existence of N-H (397.7 eV) and M-N group (397.9-398.8 eV, Figure S4, ESI).[11,33,34] The porosity and specific surface area were evaluated by N_2 adsorption-desorption isotherms (Figure S5, Table S1, ESI). Triangular micropore and hexagonal mesopore are exhibited, consistent with the reported ones in the literature.[22] The existence of mesopores is verified to facilitate the transfer of reactant and product during the electrocatalysis process.

The UV spectra of the free ligands (H_2-TCPP and M-TCPP) and the corresponding MOFs were investigated to clarify the electronic structure of each catalyst (Figure S6, ESI). As for the strong absorption of the Soret band (320-480 nm) in each free ligand, the ones in the extended frameworks are all blue-shifted, except that of PCN-222(Mn), which is red-shifted (Figure S6a-e). In general, the metal center accepts lone-pair electrons from the porphyrin ring (forming σ bonding M←N). At the same time, orbital overlapping happens between the metal center (3d) and the porphyrin ring (forming backbonding π). Therefore, electron flows easily within the delocalized π system.[35,36] If the σ bonding exerts a more potent influence than that of the backbonding π, the electronic transition on the porphyrin ring will require higher energy, which leads to a blue-shift of the Soret band and vice versa.

The formation of the extended MOF structure facilitates the

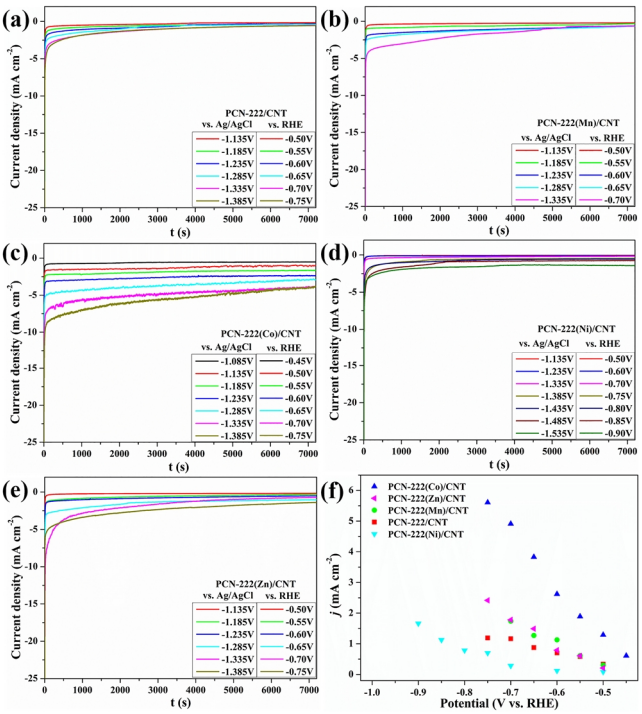

Figure 2. Chronoamperograms recorded for 2 h at various potentials in 0.5 M $KHCO_3$ aqueous solution: (a) PCN-222/CNT; (b) PCN-222(Mn)/CNT; (c) PCN-222(Co)/CNT; (d) PCN-222(Ni)/CNT; (e) PCN-222(Zn)/CNT; (f) Plotting of the average current density versus potential for each catalyst.

enhancement of symmetry. The Soret bands in PCN-222(M) and PCN-222 exhibit blue-shift (λ = 387, 366, 347, and 353 nm, respectively for Co, Ni, Zn, and metal-free) compared with the free ligand except for PCN-222(Mn) (λ = 463 nm), which exhibits a little red-shift. When compared with the metal-free PCN-222, they are all red-shifted in PCN-222(Mn), PCN-222(Co), and PCN-222(Ni), among which it shifts the most for Mn-center. This fact is probably due to the big radius of Mn^{3+} (0.58 Å) and the ligand axial coordination role of Cl, resulting in a weaker ability of binding with electrons and a high tendency of electron transport from Mn 3d to the porphyrin ring. As a result, increasing electron-cloudy in the latter would reduce the required energy for electronic transition (Figure S6f, ESI). The Zn metal insertion into the core of PCN-222 (λ = 353 nm) displays a blue-shifted Soret band (λ = 347 nm). These results hint that the metal center has a specific effect on the electronic transition in each MOF and, therefore, would cause different CO_2RR catalytic activities.

Characterizations of PCN-222/CNT and PCN-222(M)/CNT. According to our previous investigation, the composite catalysts were prepared at a ratio of PCN-222/PCN-222(M):CNT = 1:30. The PXRD for the composite was examined, as shown in Figure 1a, indicating the main contribution of CNT. A faint diffraction peak belonging to MOFs at 7.1° can be detected. The pristine MOFs show rod-like morphology, and the composite displays the fibrous character of CNT (taking the PCN-222(Co) and PCN-222(Co)/CNT as examples, Figure 1b-1c). The element mapping result of PCN-

DOI: 10.14102/j.cnki.0254-5861.2022-0057

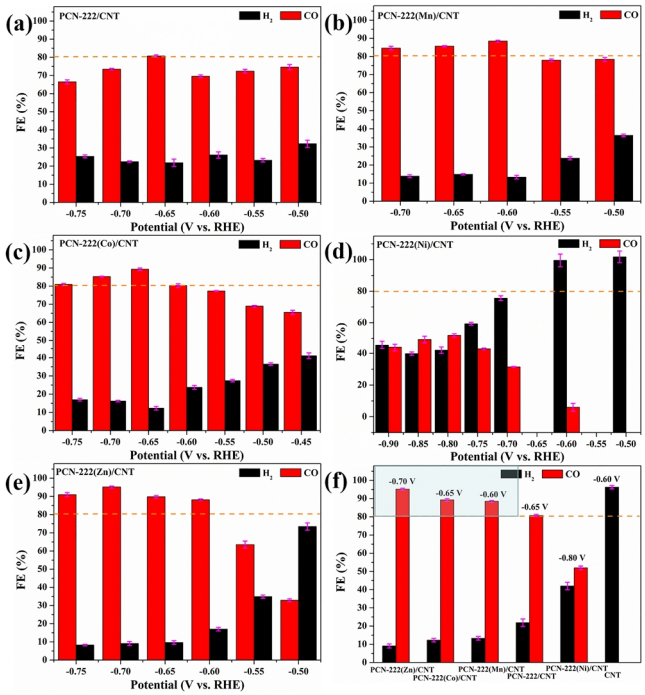

Figure 3. Faradaic efficiencies of (a) PCN-222/CNT; (b) PCN-222(Mn)/CNT; (c) PCN-222(Co)/CNT; (d) PCN-222(Ni)/CNT; (e) PCN-222(Zn)/CNT; (f) Faradaic efficiencies of each catalyst at the optimal potential.

222(Co)/CNT (Figure 1d) shows that C, N, and O elements are evenly distributed on the surface of CNT. The Co element is almost unobservable (Figure S7, ESI), indicating that the low content of PCN-222(Co) is loaded on the surface of CNT. The successful loading of extended molecular catalyst on CNT is also supported by the IR spectra characterization, on which both of the characteristic peaks of -OH (from CNT) and carboxylic groups (from MOF) are exhibited (Figure S8, ESI).

Electrochemical Performance Test. The PCN-222/CNT and PCN-222(M)/CNT modified electrodes were tested by linear sweep voltammetry (LSV) in the N_2- or CO_2-saturated 0.5 M $KHCO_3$ solution, respectively (Figure S9, ESI). The reduction potential appears earlier in the CO_2-saturated solution than in the N_2-saturated one for all catalysts. Taking PCN-222/CNT as an example, a higher current density of 37.7 mA cm^{-2} is shown at the same potential (-1.80 V vs. Ag/AgCl) in the former, and 27.5 mA cm^{-2} is observed in the latter, indicating that CO_2 is catalyzed.[37] Moreover, the combination with CNT can significantly improve the conductivity of the catalyst and generate considerable catalytic effects even with low catalyst loading, which is proved by comparing CV curves to the electrodes made by mixing with active carbon in 1:2 (Figure S10, ESI). The composite catalysts (PCN-222(M)/CNT and PCN-222/CNT) also show a more positive reduction potential and higher current density than CNT alone (Figure S11, ESI).[38]

The electrolysis experiments were performed at various potentials for 2 h from -0.50 to -0.75 V vs. RHE (Figure 2), showing a noticeable difference in the current density at different metal-porphyrin centers. The average density versus potential is plotted in Figure 2f. The PCN-222(Co)/CNT composite shows the highest current density, while PCN-222(Mn)/CNT and PCN-222(Zn)/CNT are slightly inferior but considerably higher than that of PCN-222/CNT at higher potential. The PCN-222(Ni)/CNT composite exhibits a much lower current density than the others in the same potential range of -0.50 to -0.75 V vs. RHE. The Faraday efficiencies (FE) of the gas products for each catalyst electrolyzed at different potentials are shown in Figure 3. Hydrogen and carbon monoxide are the main products with all the catalysts, but CO_2RR activity is dependent on the metal center in each one (Table S2-S6, ESI). As for PCN-222/CNT composite, it exhibits moderate CO_2RR activity that FE_{CO} maintains at 60%-80%, and FE_{H2} lies in 20%-35% (FE_{COmax} = 80.7%, j = 0.9 mA cm^{-2}, -0.65 V vs. RHE). PCN-222(M)/CNT (M = Mn, Co, Zn) displays much higher catalytic activity (FE_{CO} > 80%) than PCN-222/CNT from -0.60 to -0.70 V vs. RHE. Especially for PCN-222(Mn)/CNT (FE_{COmax} = 88.5%, j = 1.1 mA cm^{-2}, -0.60 V vs. RHE, η = 494 mV) and PCN-222(Co)/ CNT (FE_{COmax} = 89.3%, j = 3.8 mA cm^{-2}, -0.65 V vs. RHE, η = 544 mV), they are featured with low overpotential and high current density, respectively, for reaching a high $CO_2 \rightarrow CO$ conversion efficiency. PCN-222(Zn)/CNT presents a higher selectivity to CO, with 92.5% of FE_{COmax} (j = 1.8 mA cm^{-2}, -0.70 V vs. RHE) with a bigger overpotential 594 mV. To our surprise, PCN-222(Ni)/CNT exhibits better activity towards the hydrogen evolution reaction (HER), while the

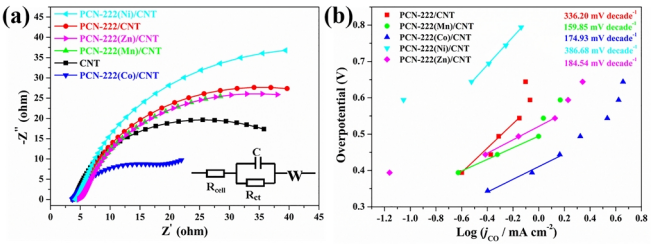

Figure 4. (a) Nyquist plot at -0.6 V vs. RHE and (b) Tafel plot for CO of each catalyst.

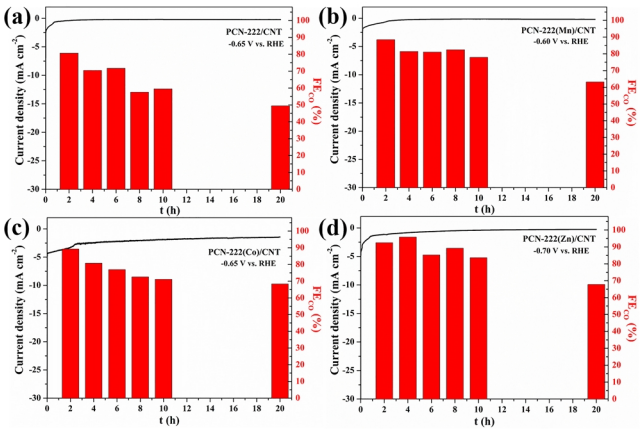

Figure 5. Long-term chronoamperometry test (20 h) and Faradaic efficiency for CO as a function of time for each catalyst: (a) PCN-222/CNT; (b) PCN-222(Mn)/CNT; (c) PCN-222(Co)/CNT; (d) PCN-222(Zn)/CNT.

Chin. J. Struct. Chem. **2022**, 41, 2207046-2207052
DOI: 10.14102/j.cnki.0254-5861.2022-0057

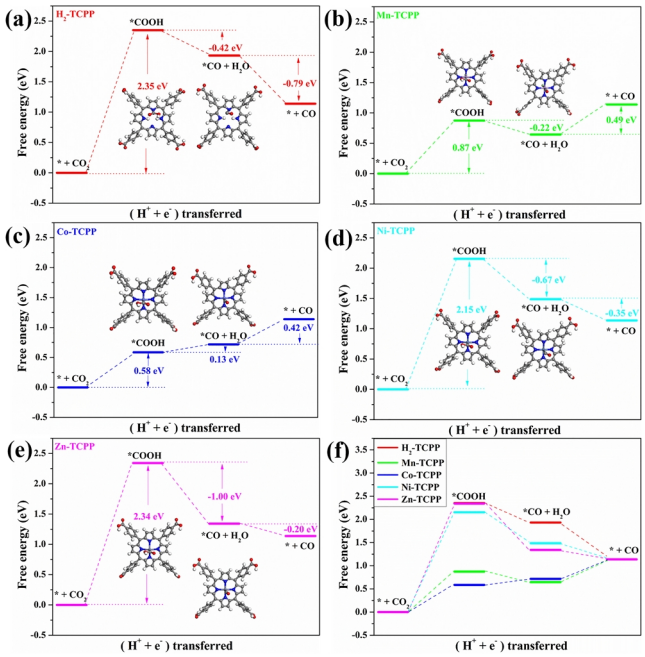

Figure 6. The free energy diagrams of CO_2 reduction to CO for (a) PCN-222/CNT; (b) PCN-222(Mn)/CNT; (c) PCN-222(Co)/CNT; (d) PCN-222(Ni)/CNT; (e) PCN-222(Zn)/CNT; (f) Comparisons of free energy for each catalyst.

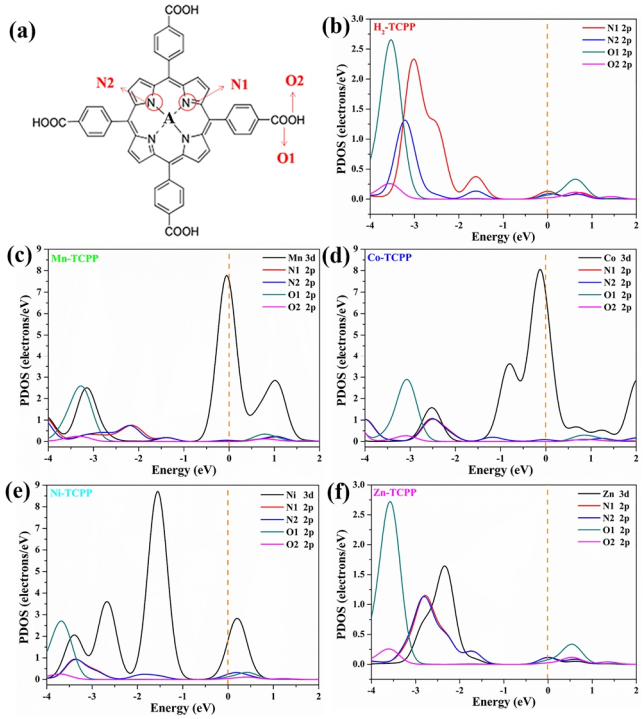

Figure 7. (a) Illustration of the configuration of A-TCPP (A = H_2, Mn, Co, Ni, Zn) with different N, O environments; the PDOS of (b) H_2-TCPP; (c) Mn-TCPP; (d) Co-TCPP; (e) Ni-TCPP; (f) Zn-TCPP.

FE_{COmax} (52.0%) is even less than that of PCN-222/CNT at -0.80 V vs. RHE (j = 0.8 mA cm^{-2}). Moreover, under low overpotential, it displays almost 100% FE_{H2} but much slight current density (j < 0.1 mA cm^{-2}). The blank experiment for pure CNT was also performed, exhibiting the entire H_2 product (-0.60 V vs. RHE, FE_{H2} = 96.2%, Table S7, ESI).

The CO_2RR activity-metal center correlation hints that the current density plays an essential role in the highly efficient transformation of CO_2 to CO. Therefore, we investigated the electrochemically active area (ECSA, Figure S12, ESI) and electrochemical impedance spectroscopy (EIS) of each catalyst (Figure 4a). PCN-222(M)/CNT (M = Mn, Co, Zn) all behave with higher ECSA (763.5, 740.0, and 775.5 cm^2, respectively, Table S8, ESI), and lower charge transfer resistance (R_{ct} = 37.2, 10.4 and 39.6 Ω, Table S9, ESI), indicating their effective electrochemical area for electrocatalysis[27,38] and faster charge transfer rate,[37,39] which are superior to that of PCN-222/CNT (628.5 cm^2, 44.0 Ω). In contrast, PCN-222(Ni)/CNT presents a flawed character (647.0 cm^2, 61.3 Ω).

The reaction kinetics for the CO formation is elucidated by the Tafel slopes based on j-η data (Figure 5b). Remarkably, the slopes for PCN-222(Mn)/CNT, PCN-222(Co)/CNT, and PCN-222(Zn)/CNT are 159.85, 174.93, and 184.54 mV $decade^{-1}$, respectively, suggesting the faster kinetics for the CO formation,[27,40] which are significantly lower than that of PCN-222/CNT (336.20 mV $decade^{-1}$) and PCN-222(Ni)/CNT (386.68 mV $decade^{-1}$).

We also performed the long-time durability tests (20 h) for each catalyst at its optimal potential to evaluate the stability (Figure 5, Figure S13, ESI). The corresponding FE_{CO} can be retained at >70% within 10 h for PCN-222(Mn)/CNT, PCN-222(Co)/CNT, and PCN-222(Zn)/CNT (Table S10, ESI). In contrast, the FE_{CO} of PCN-222/CNT drops to 59.5%. The substantial stability of PCN-222(M)/CNT (M = Mn, Co, Zn) guarantees their efficient electrocatalytic transformation of CO_2 to CO. In comparison to some heterogeneous catalysts with M-N_x centers, the composites of PCN-222(M)/CNT (M = Mn, Co, Zn) behave remarkable advantages in both CO_2→CO efficiency and overpotential (Table S11, ESI).

DFT Calculation of PCN-222 and PCN-222(M). To clarify the role of metal centers in PCN-222(M) for CO_2RR, we chose the free ligands of H_2-TCPP and M-TCPP (M = Mn^{III}, Co^{II}, Ni^{II}, Zn^{II}), as the models to perform density functional theoretical (DFT) calculations (the detailed calculation process is listed in ESI). In general, three steps are involved during the CO_2→CO process: the formation of *COOH and *CO, and the final CO desorption.[41] Based on the calculated free energy result, for CO_2RR in each model, the initial proton-coupled electron transfer of CO_2 to form the *COOH intermediate is sluggish, indicating the rate-determining step (RDS) is the formation of *COOH (Figure 6). Mn-TCPP and Co-TCPP possess a much smaller free energy of ΔG_{*COOH} (0.87 and 0.58 eV, respectively), being consistent with the high catalytic activity and selectivity of PCN-222(Mn)/CNT and PCN-222(Co)/CNT. H_2-TCPP and Zn-TCPP possess similar ΔG_{*COOH} of 2.35 and 2.34 eV, respectively, slightly higher than Ni-TCPP (2.15 eV).

Since the CO_2RR process involves the electron transfer and the central metal ions would affect the distribution of frontier molecular orbital, we further investigated each catalyst's HOMO and LUMO orbital energies and its 1e^- reduced form (Table S12-13,

DOI: 10.14102/j.cnki.0254-5861.2022-0057

ESI). As reported, the frontier molecular orbital is closely related to the redox potential of each catalyst, and the HOMO-LUMO gap (ΔE_{L-H}) should account for the electrocatalytic reduction ability. Mn-TCPP and Co-TCPP display lower ΔE_{L-H} of 0.036 and 0.057 eV, respectively, further decreasing to 0.023 and 0.024 eV, respectively, after another electron acquisition. They also exhibit good conductivity and efficient internal electron transfer, confirmed by the partial density of states (PDOS) result (Figure 7c, d).[25] The PDOS near the Fermi level of their reduced form is dominated by Mn/Co 3d and N1-2p states, with gaps of 0.01 and 0.09 eV, respectively, indicating the high density of carriers near the Fermi level.[42,43] However, although Ni-TCPP exhibits a small band peak gap of 0.02 eV, the contribution of the Ni-3d state is much less than that of Mn-TCPP/Co-TCPP, hinting at the low density of carriers near the Fermi level and low conductivity (Figure 7e). Such electronic structural feature, together with the higher ΔE_{L-H} value of 0.060 eV (0.055 eV for $1e^-$ reduction), should account for the insufficient CO_2RR activity of PCN-222(Ni)/CNT.

As for H_2-TCPP and Zn-TCPP, they display similar ΔE_{L-H} gaps of 0.062 and 0.066 eV (0.060 and 0.063 eV for $1e^-$ reduction), but the Zn insertion contributes to decreasing the band peak gap. Different from those of Mn-TCPP/Co-TCPP/Ni-TCPP, the PDOS near the Fermi level of H_2-TCPP and Zn-TCPP is determined by the contribution of two types of N-2p states (N1, N2) in the porphyrins, with the gaps of 0.05 eV and close to zero, respectively (Figure 7b, f). This fact indicates that the active sites are concentrated on the N atoms in the porphyrin ring in each model, while the Zn center is essential for increasing electron mobility in the porphyrin ring.[44-46] Therefore, the maximum FE_{CO} for PCN-222(Zn)/CNT is significantly higher than PCN-222/CNT.

Based on the experimental results and theoretical calculations, we seem to get the correlation between structure and performance. The strength of the backbonding π of the transition metal and its influence on the electron mobility in the porphyrin ring can affect its CO_2RR activity. The high electron-cloud density and good electron mobility of the porphyrin ring would help improve its activity ($CO_2 \rightarrow CO$), such as Mn-TCPP, Co-TCPP, and Zn-TCPP. It should be stressed that the coordination environment around the metal center ($Mn^{III}N_4Cl$) would also have an influence on the CO_2RR activity.[47]

n CONCLUSION

In summary, this work employed PCN-222(M)/CNT (M = Mn, Co, Ni, Zn) with a clear M-N_4 structure as model catalysts and explored the structure-activity relationship between the metal center and CO_2RR through the combination of theoretical calculation and experimental results. We found that PCN-222(Mn)/CNT, PCN-222(Co)/CNT, and PCN-222(Zn)/CNT composite materials exhibit high catalytic activity for CO_2RR, with the FE_{COmax} of 88.5%, 89.3%, and 92.5%, respectively. They display fast kinetics for the CO formation, with the Tafel slopes of 159.85, 174.93, and 184.54 mV $decade^{-1}$, respectively. The metal center in M-N_4 with stronger backbonding π strength and higher electron-cloud density is more conducive to improving the $CO_2 \rightarrow CO$ activity. This work provides new ideas for exploring catalysts with high catalytic activity, which would be suggestive for further research.

n EXPERIMENTAL

Synthesis of PCN-222 and PCN-222(M). PCN-222 and PCN-222(M) were synthesized according to a process described in the literature.[22]

Synthesis of PCN-222/CNT and PCN-222(M)/CNT. Take the synthesis of PCN-222/CNT as an example. $ZrCl_4$ (70.0 mg), tetrakis(4-carboxyphenyl)-porphyrin (H_2-TCPP, 50.0 mg), benzoic acid (2.7 g), and hydroxylated CNTs (1.5 g) were dissolved in 8.0 mL DMF and were placed in a polytetrafluoroethylene autoclave. The mixture was maintained at 120 ºC for 48 h. Then, the dark sample was harvested by filtration, followed by acid treatment for 12 h (8.0 M HCl). The obtained material was washed with DMF and acetone, respectively. According to the above-mentioned method, PCN-222(M)/CNT composite materials were synthesized when replacing H_2-TCPP with M-TCPP in each process.

n ACKNOWLEDGEMENTS

This work was financially supported by the NNSFC (No. 21671169), and the Foundation from the Priority Academic Program Development of Jiangsu Higher Education Institutions.

n AUTHOR CONTRIBUTIONS

Mengjie Liu and Mengting Peng contributed equally to this work.

n AUTHOR INFORMATION

Corresponding authors. Emails: bxdong@yzu.edu.cn and qxuchem@yzu.edu.cn

n COMPETING INTERESTS

The authors declare no competing interests.

n ADDITIONAL INFORMATION

Supplementary information is available for this paper at http://manu30.magtech.com.cn/jghx/EN/10.14102/j.cnki.0254-5861.2022-0057

For submission: https://mc03.manuscriptcentral.com/cjsc

n REFERENCES

(1) Porosoff, M. D.; Yan, B.; Chen, J. G. Catalytic reduction of CO_2 by H_2 for synthesis of CO, methanol and hydrocarbons: challenges and opportunities. *Energy Environ. Sci.* **2016**, 9, 62-73.

(2) Jiang, J.; Wu, Q.; Huang, Y. B.; Cao, R. Reticular frameworks and their derived materials for CO_2 conversion by thermo-catalysis. *EnergyChem* **2021**, 3, 100064.

(3) Bhatia, S. K.; Bhatia, R. K.; Jeon, J. M.; Kumar, G.; Yang, Y. H. Carbon dioxide capture and bioenergy production using biological system – a review. *Renew. Sust. Energy Rev.* **2019**, 110, 143-158.

(4) Hussain, I.; Jalil, A. A.; Hassan, N. S.; Hamid, M. Y. S. Recent advances in catalytic systems for CO_2 conversion to substitute natural gas (SNG): perspective and challenges. *J. Energy Chem.* **2021**, 62, 377-407.

(5) Benson, E. E.; Kubiak, C. P.; Sathrum, A. J.; Smieja, J. M. Electrocatalytic and homogeneous approaches to conversion of CO_2 to liquid fuels. *Chem. Soc. Rev.* **2009**, 38, 89-99.

(6) Qiao, J. L.; Liu, Y. Y.; Hong, F.; Zhang, J. J. A review of catalysts for the electroreduction of carbon dioxide to produce low-carbon fuels. *Chem. Soc.*

DOI: 10.14102/j.cnki.0254-5861.2022-0057

Rev. **2014**, 43, 631-675.
(7) Zhang, W. J.; Hu, Y.; Ma, L. B.; Zhu, G. Y.; Wang, Y. R.; Xue, X. L.; Chen, R. P.; Yang, S. Y.; Jin, Z. Progress and perspective of electrocatalytic CO_2 reduction for renewable carbonaceous fuels and chemicals. *Adv. Sci.* **2018**, 5, 1700275(1-24).
(8) Zhang, M. D.; Dong, Y. J.; Huang, Y. B.; Cao, R. Covalent triazine frameworks-derived N, P dual-doped porous carbons for highly efficient electrochemical reduction of CO_2. *Chin. J. Struct. Chem*. **2021**, 40, 1213-1222.
(9) Paul, S.; Kao, Y. L.; Ni, L. M.; Ehnert, R.; Geppert, I. H.; Krol, R.; Stark, R. W.; Jaegermann, W.; Kramm, U. I.; Bogdanoff, P. Influence of the metal center in M-N-C catalysts on the CO_2 reduction reaction on gas diffusion electrodes. *ACS Catal*. **2021**, 11, 5850-5864.
(10) Wang, F. Y.; Liu, Y.; Song, Z. L.; Miao, Z. C.; Zhao, J. P. Ni-N-doped carbon-modified reduced graphene oxide catalysts for electrochemical CO_2 reduction reaction. *Catal*. **2021**, 11, 561.
(11) Varela, A. S.; Ju, W.; Bagger, A.; Franco, P.; Rossmeisl, J.; Strasser, P. Electrochemical reduction of CO_2 on metal-nitrogen-doped carbon catalysts. *ACS Catal*. **2019**, 9, 7270-7284.
(12) Ju, W.; Bagger, A.; Hao, G. P.; Varela, A. S.; Sinev, I.; Bon, V.; Roldan, C. B.; Kaaskel, S.; Rossmeisl, J.; Strasser, P. Understanding activity and selectivity of metal-nitrogen-doped carbon catalysts for electrochemical reduction of CO_2. *Nat. Commun*. **2017**, 8, 944-952.
(13) Ren, S. X.; Joulié, D.; Salvatore, D.; Torbensen, K.; Wang, M.; Robert, M.; Berlinguette, C. P. Molecular electrocatalysts can mediate fast, selective CO_2 reduction in a flow cell. *Science* **2019**, 365, 367-369.
(14) Meng, D. L.; Zhang, M. D.; Si, D. H.; Mao, M. J.; Hou, Y.; Huang, Y. B.; Cao, R. Highly selective tandem electroreduction of CO_2 to ethylene over atomically isolated nickel-nitrogen site/copper nanoparticle catalysts. *Angew. Chem. Int. Ed*. **2021**, 60, 25485-25492.
(15) Hou, Y.; Huang, Y. B.; Liang, Y. L.; Chai, G. L.; Yi, J. D.; Zhang, T.; Zang, K. T.; Luo, J.; Xu, R.; Lin, H.; Zhang, S. Y.; Wang, H. M.; Cao, R. Unraveling the reactivity and selectivity of atomically isolated metal-nitrogen sites anchored on porphyrinic triazine frameworks for electroreduction of CO_2. *CCS Chem*. **2019**, 1, 384-395.
(16) Hu, X. M.; Rønne, M. H.; Pedersen, S. U.; Skrydstrup, T.; Daasbjerg, K. Enhanced catalytic activity of cobalt porphyrin in CO_2 electroreduction upon immobilization on carbon materials. *Angew. Chem. Int. Ed*. **2017**, 56, 6468-6472.
(17) Weng, Z.; Jiang, J. B.; Wu, Y. S.; Wu, Z. S.; Guo, X. T.; Materna, K. L.; Liu, W.; Batista, V. S.; Brudvig, G. W.; Wang, H. L. Electrochemical CO_2 reduction to hydrocarbons on a heterogeneous molecular Cu catalyst in aqueous solution. *J. Am. Chem. Soc*. **2016**, 138, 8076-8079.
(18) Yan, T. T.; Guo, J. H.; Liu, Z. Q.; Sun, W. Y. Metalloporphyrin encapsulation for enhanced conversion of CO_2 to C_2H_4. *ACS Appl. Mater. Interfaces* **2021**, 13, 25937-25945.
(19) Watpathomsub, S.; Luangchaiyaporn, J.; Sariciftci, N. S.; Thamyongkit, P. Efficient heterogeneous catalysis by pendant metalloporphyrin-functionalized polythiophenes for the electrochemical reduction of carbon dioxide. *New J. Chem*. **2020**, 44, 12486-12495.
(20) Zhou, H. C.; Kitagawa, S. Metal-organic frameworks (MOFs). *Chem. Soc. Rev.* **2014**, 43, 5415-5418.
(21) Bai, Y.; Dou, Y. B.; Xie, L. H.; Rutledge, W.; Li, J. R.; Zhou, H. C. Zr-based metal-organic frameworks: design, synthesis, structure, and applications. *Chem. Soc. Rev*. **2016**, 45, 2327-2367.
(22) Feng, D. W.; Gu, Z. Y.; Li, J. R.; Jiang, H. L.; Wei, Z. W.; Zhou, H. C. Zirconium-metalloporphyrin PCN-222: mesoporous metal-organic frameworks with ultrahigh stability as biomimetic catalysts. *Angew. Chem. Int. Ed*. **2012**, 51, 10307-10310.
(23) Feng, D. W.; Jiang, H. L.; Chen, Y. P.; Gu, Z. Y.; Wei, Z. W.; Zhou, H. C. Metal-organic frameworks based on previously unknown Zr_8/Hf_8 cubic clusters. *Inorg. Chem*. **2013**, 52, 12661-12667.
(24) Feng, D. W.; Chung, W. C.; Wei, Z. W.; Gu, Z. Y.; Jiang, H. L.; Chen, Y. P.; Darensbourg, D. J.; Zhou, H. C. Construction of ultrastable porphyrin Zr metal-organic frameworks through linker elimination. *J. Am. Chem. Soc*. **2013**, 135, 17105-17110.
(25) Wang, Y. R.; Huang, Q.; He, C. T.; Chen, Y. F.; Liu, J.; Shen, F. C.; Lan, Y. Q. Oriented electron transmission in polyoxometalate-metalloporphyrin organic framework for highly selective electroreduction of CO_2. *Nat. Commun*. **2018**, 9, 4466-4473.
(26) Ahrenholtz, S. R.; Epley, C. C.; Morris, A. J. Solvothermal preparation of an electrocatalytic metalloporphyrin MOF thin film and its redox hopping charge-transfer mechanism. *J. Am. Chem. Soc*. **2014**, 136, 2464-2472.
(27) Hod, I.; Sampson, M. D.; Deria, P.; Kubiak, C. P.; Farha, O. K.; Hupp, J. T. Fe-porphyrin-based metal-organic framework films as high-surface concentration, heterogeneous catalysts for electrochemical reduction of CO_2. *ACS Catal*. **2015**, 5, 6302-6309.
(28) Xin, Z. F.; Wang, Y. R.; Chen, Y. F.; Li, W. L.; Dong, L. Z.; Lan, Y. Q. Metallocene implanted metalloporphyrin organic framework for highly selective CO_2 electroreduction. *Nano Energy* **2020**, 67, 104233.
(29) Dong, B. X.; Qian, S. L.; Bu, F. Y.; Wu, Y. C.; Feng, L. G.; Teng, Y. L.; Liu, W. L.; Li, Z. W. Electrochemical reduction of CO_2 to CO by a heterogeneous catalyst of Fe-porphyrin-based metal-organic framework. *ACS Appl. Energy Mater.* **2018**, 1, 4662-4669.
(30) Liu, M. J.; Cao, S. M.; Feng, B. Q.; Dong, B. X.; Ding, Y. X.; Zheng, Q. H.; Teng, Y. L.; Li, Z. W.; Liu, W. L.; Feng, L. G. Revealing the structure-activity relationship of two Cu-porphyrin-based metal-organic frameworks for the electrochemical CO_2-to-HCOOH transformation. *Dalton Trans*. **2020**, 49, 14995-15001.
(31) Kung, C. W.; Goswami, S.; Hod, I.; Wang, T. C.; Duan, J. X.; Farha, O. K.; Hupp, J. T. Charge transport in zirconium-based metal-organic frameworks. *Acc. Chem. Res*. **2020**, 53, 1187-1195.
(32) Maindan, K.; Li, X. L.; Yu, J. R.; Deria, P. Controlling charge-transport in metal-organic frameworks: contribution of topological and spin-state variation on the iron-porphyrin centered redox hopping rate. *J. Phys. Chem. B* **2019**, 123, 8814-8822.
(33) Wang, F. Y.; Liu, Y.; Song, Z. L.; Miao, Z. C.; Zhao, J. P. Ni-N-doped carbon-modified reduced graphene oxide catalysts for electrochemical CO_2 reduction reaction. *Catal*. **2021**, 11, 561.
(34) Matanovic, I.; Babanova, S.; Perry III, A.; Serov, A.; Artyushkova, K.; Atanassov, P. Bio-inspired design of electrocatalyst for oxalate oxidation: a combined experimental and computational study of Mn-N-C catalysts. *Phys. Chem. Chem. Phys*. **2015**, 17, 13235-13244.
(35) Wang, L. Z.; She, Y. B. Spectroscopic analysis of substituted tetraphenylporphyrin iron, manganese, cobalt, copper and zinc complexes. *Spectrosc. Spect. Anal*. **2008**, 28, 2312-2317.
(36) Soldatova, A. V.; Ibrahim, M.; Spiro, T. G. Electronic structure and ligand vibrations in FeNO, CoNO, and FeOO porphyrin adducts. *Inorg. Chem.* **2013**, 52, 7478-7486.
(37) Cao, C. S.; Ma, D. D.; Gu, J. F.; Xie, X. Y.; Zeng, G.; Li, X. F.; Han, S. G.; Zhu, Q. L.; Wu, X. T.; Xu, Q. Metal-organic layers leading to atomically thin bismuthene for efficient carbon dioxide electroreduction to liquid fuel.

DOI: 10.14102/j.cnki.0254-5861.2022-0057

Angew. Chem. Int. Ed. **2020**, 59, 15014-15020.

(38) Chen, E. X.; Yang, J.; Qiu, M.; Wang, X. Y.; Zhang, Y. F.; Guo, Y. J.; Huang, S. L.; Sun, Y. Y.; Zhang, J.; Hou, Y.; Lin, Q. P. Understanding the efficiency and selectivity of two-electron production of metalloporphyrin-embedded zirconium-pyrogallol scaffolds in electrochemical CO_2 reduction. *ACS Appl. Mater. Interfaces* **2020**, 12, 52588-52594.

(39) Jadhav, H. S.; Roy, A.; Thorat, G. M.; Chung, W. J.; Seo, J. G. Hierarchical free-standing networks of $MnCo_2S_4$ as efficient electrocatalyst for oxygen evolution reaction. *J. Ind. Eng. Chem*. **2019**, 71, 452-459.

(40) Han, N.; Wang, Y.; Ma, L.; Wen, J. G.; Li, J.; Zheng, H. C.; Nie, K. Q.; Wang, X. X.; Zhao, F. P.; Li, Y. F.; Fan, J.; Zhong, J.; Wu, T. Q.; Miller, D. J.; Lu, J.; Lee, S. T.; Li, Y. G. Supported cobalt polyphthalocyanine for high-performance electrocatalytic CO_2 reduction. *Chem* **2017**, 3, 652-664.

(41) Cheng, Q. Q.; Mao, K.; Ma, L. S.; Yang, L. J.; Zou, L. L.; Zou, Z. Q.; Hu, Z.; Yang, H. Encapsulation of iron nitride by Fe-N-C shell enabling highly efficient electroreduction of CO_2 to CO. *ACS Energy Lett*. **2018**, 3, 1205-1211.

(42) Arriagada, D. C.; Rojas, S. M.; Mora, F. C.; Labbé, A. T. First-principles study of hybrid nanostructures formed by deposited phthalocyanine/porphyrin metal complexes on phosphorene. *J. Mol. Liq*. **2021**, 333, 115948-11557.

(43) Wang, C.; Zhu, C. Y.; Zhang, M.; Geng, Y.; Li, Y. G.; Su, Z. M. An intriguing window opened by a metallic two-dimensional lindqvist-cobaltporphyrin organic framework as an electrochemical catalyst for the CO_2 reduction reaction. *J. Mater. Chem. A* **2020**, 8, 14807-14814.

(44) Wu, Y. S.; Jiang, J. B.; Weng, Z.; Wang, M. Y.; Broere, D. L. J.; Zhong, Y. R.; Brudvig, G. W.; Feng, Z. X.; Wang, H. L. Electroreduction of CO_2 catalyzed by a heterogenized Zn-porphyrin complex with a redox-innocent metal center. *ACS Cent. Sci.* **2017**, 3, 847-852.

(45) Cao, M. J.; Yu, Y. M.; Fu, H. Y.; She, Y. B. Effect of substituents and central metal ions on electronic structure and catalytic activity of porphyrins. *CIESC J*. **2013**, 64, 88-97.

(46) Wu, H.; Fan, S. H.; Zhang, H.; Li, H. Q.; Yang, M. Q.; Zhang, C. Y. Porphyrins with different electron groups: spectral and DFT study. *Spectrosc. Spect. Anal*. **2014**, 34, 1060-1063.

(47) Yan, T. T.; Wang, P.; Xu, Z. H.; Sun, W. Y. Copper(II) frameworks with varied active site distribution for modulating selectivity of carbon dioxide electroreduction. *ACS Appl. Matter. Interfaces* **2022**, 14, 13645-13652.

Received: March 16, 2022
Accepted: April 4, 2022
Published online: April 15, 2022
Published: July 18, 2022

DOI: 10.14102/j.cnki.0254-5861.2022-0057